Characterization and Modeling of Symmetric and Asymmetric Damping Properties of a Magnetorheological Damper

EN-RONG WANG WAN-JUN WANG HUI WANG
School of Electrical & Automation Engineering
Nanjing Normal University
No. 78 Ban-cang Street, Nanjing 210042, CHINA
http://d.njnu.edu.cn/newshtml/lishi/20050116131230.htm

SUBHASH RAKHEJA CHUN-YI SU
Department of Mechanical & Industrial Engineering
Concordia University
Montreal, CANADA H3G 1M8

Abstract: - For realizing the intelligent vehicle suspension design with magneto-rheological (MR) fluids dampers, extensive laboratory measurements are performed to characterize the symmetric and asymmetric hysteresis force properties of a MR-damper, under a wide range of drive current and harmonic excitation conditions (frequency and stroke). The proposed asymmetric damping force generation (ADFG) algorithm is employed to generate the asymmetric damping force in compression and extension for the symmetry MR-damper, and a generalized model is proposed to characterize the symmetric and asymmetric hysteretic force-velocity (*f-v*) characteristics of the controllable MR-damper. The measured data are used to identify the symmetric and asymmetric hysteretic *f-v* model parameters, and simulations are performed to assess the effectiveness of the proposed model synthesis by comparing the results with those obtained from the measured data under wide range of operating conditions. The results show reasonably good agreements between the simulation results and the measured data, irrespective of the excitation conditions and control current, and verify that the proposed ADFG algorithm is essential to yield the asymmetric damping property from the symmetry MR-damper.

Key-Words: - Magneto-rheological fluids damper Characteristics Hardware-in–the-loop test Characterization Modeling

1 Introduction

A wide range of magneto-rheological (MR) fluid-based dampers are currently being explored for their potential implementation in various systems, such as vibration control devices and vehicle suspension. A number of analytical and experimental studies have clearly established superior potential performance benefits of the MR-damper in vehicle applications in relation to conventional hydraulic dampers[1-3]. The MR dampers offer high viscous damping corresponding to low velocities in the pre-yield condition, while the post-yield saturation corresponding to high velocities can be characterized by a considerably lower viscous damping coefficient. The requirement of adequate ride, road-holding, handling and directional control stability performance of road vehicles entails variable damping, which could be achieved with MR dampers with only minimal power consumption, unlike a fully active suspension which could add or remove energy depending upon the demand with the help of an elaborate power supply[4]. The semi-actively controlled MR-fluid dampers offer rapid variations in damping properties in a reliable fail-safe manner, since they continue to provide adequate damping in a passive manner in the event of control hardware malfunction[5]. Although a vast number of semi-active variable damping concepts based upon hydraulic flows modulation and electro-rheological (ER) fluids have been developed, definite advantages of the MR-fluid dampers have been clearly established, such as significantly higher yield stress and wider operating temperature[3]. Owing to the rheology of MR-fluid in terms of its shear stress-strain rate behavior, the damper exhibits highly nonlinear variations in damping force, attributed to the hysteresis and force-limiting properties of the fluid as functions of intensity of applied magnetic field, and displacement and velocity of the piston. The development of an effective controller for

realizing desirable variations in damping requires accurate characterization of hysteretic force-velocity (*f-v*) characteristics of the MR-damper in the pre-yield condition and force saturation in the post-yield condition. Spencer, et al[2], proposed a damper model on the basis of the Bouc-Wen hysteresis model. The model, however, poses inherent difficulties in predicting essential parameters and in realizing control systems for desired tracking control performance. Bingham plastic model has been proposed assuming rigid material behavior in the pre-yield, while the shear flow in the post-yield is characterized by a viscous damping coefficient. Assuming the material to be plastic in both pre- and post-yield conditions, Stanway, et al[1], proposed a nonlinear model, where the pre-yield force is characterized by considerably high viscous damping. On the basis of this model, Wereley, et al[3], proposed a nonlinear hysteretic bilinear model by fitting the *f-v* characteristics using four parameters: pre- and post-yield viscous damping coefficients, yield force and zero-force velocity intercept. The above models, however, do not include the effects of continually varying control current. Moreover, hysteretic damping force generated by a MR-damper not only depends upon the intensity of the magnetic field but also upon the excitation frequency and amplitude, and can only yield the symmetric damping property in compression and rebound.

In this study, extensive laboratory tests are performed to characterize the dependence of hysteretic damping force of a candidate MR-damper under a wide range of drive current and excitation conditions (frequency and stroke), so as to synthesize an optimal semi-active controller for implementing intelligent vehicle suspension with the symmetry MR-damper[6-8]. The proposed asymmetric damping force generation (ADFG) algorithm[9] is employed to modulate the drive current in asymmetric mode to generate the asymmetric damping force in compression and rebound for the symmetry MR-damper, and the proposed generalized MR-damper model[10] is proposed to characterize the hysteretic *f-v* characteristics of the controllable symmetry and asymmetry MR dampers. The generalized model synthesis in conjunction with the measured data for the symmetric and asymmetric damping characteristics are used to identify the model parameters. Simulations are performed to assess the effectiveness of the proposed model synthesis, and results obtained under wide range of simulation conditions are compared with those obtained from the measured data[11].

2 Characterization of Symmetric Hysteretic F-V Characteristics

A MR-damper, developed by CARRERA[12] and pictorially shown in Fig.1, is considered for characterizing its damping properties in the laboratory and applying in present studies[6-8]. The considered damper, designed for automotive applications, could provide a total stroke of 200 mm. The damper is a mono-tube design and comprises floating piston, which separates the MR-fluid and the gas media. The piston is designed with annular orifices, and it comprises electro-magnetic coils to generate magnetic field in response to an applied electric current. The variations in viscous and shear properties of the fluid, caused by the applied magnetic field, yield variations in the damping force developed by the damper. For this particular damper, a direct current limited to 0.5 A at 12 V serves as the command signal for the coils.

Fig.1 A pictorial view of a candidate MR-damper

2.1 Test apparatus and methodology

The force-velocity (*f-v*) and force-displacement (*f-d*) characteristics of the candidate MR-damper are measured in the laboratory over a wide range of applied currents and excitations. A voltage-to-current circuit is designed to realize different constant levels of current excitations for the coil. Owing to the symmetric design of the damper, the voltage-to-current circuit is initially applied to obtain symmetric *f-v* characteristics in compression and rebound under a fixed drive current and symmetric excitation. A Hardware-in-the-loop (HIL) test platform, as shown in Fig.2, is developed in the laboratory[8, 10]. The candidate MR-damper is installed on an MTS electro-hydraulic vibration exciter between the exciter and a fixed inertial frame through a force transducer. Position (LVDT) and velocity (LVT) sensors are also installed on the exciter to measure the instantaneous position and velocity of the damper piston. The damper is subject to harmonic displacement excitations of different constant amplitudes at selected discrete frequencies to characterize its properties over a wide range of excitations. The force, velocity and displacement

data, acquired through a data acquisition board, are directly imported into an Excel worksheet using Dynamic Data Exchange to obtain an on-line display of the hysteretic *f-v* characteristics. A dual regulated DC power supply is used to supply the command current to the damper. A thermocouple is also mounted on the damper body to monitor the damper temperature. The experimental data under each condition were acquired in the vicinity of a defined temperature range (40±10 °C), so as to suppress the thermal effects in the characterization task.

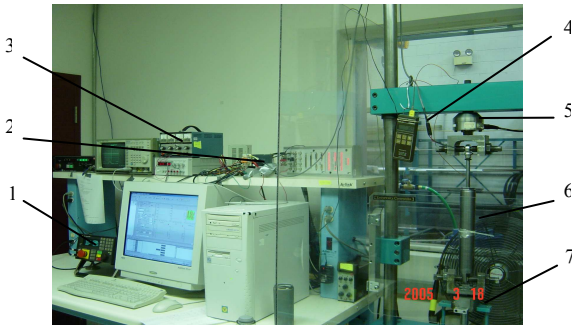

Fig.2 A pictorial view of MR-damper test system (1-Servo-controller, 2-Data acquisition, 3-DC power supply, 4-Temperature monitor, 5-Force transducer; 6-MR-damper, 7-Hydraulic actuator)

The hysteretic *f-v* characteristics of the candidate damper, symmetric in compression and rebound, are measured under sinusoidal displacement excitations at several discrete frequencies in the 0 to 15 Hz range, which is considered to represent the range of predominant vehicular motions along the vertical axis. The tests are performed under different constant magnitudes a_m of displacement, ranging from 2.5 to 75 mm, and command current i_d in the 0 to 0.4 A range. A total of 165 tests are performed corresponding to different combinations of frequency, stroke and drive current, as summarized in Table 1. The amplitudes of displacement excitations at higher frequencies are limited to lower values to ensure damper operation within safe velocity limits.

The measurements are initially performed under low amplitude excitation at a frequency of 0.1 Hz. The measured force is considered to represent the seal friction, assuming negligible contributions due to MR-fluid damping at extremely low velocities[5]. The damper is then subjected to a selected excitation condition and current using the servo-controller and the voltage-current circuit, respectively. The force, velocity and displacement signals are acquired in the dynamic state as the body temperature approaches 40°C. The measured signals are displayed in the form of time-histories and Lissajuous curves in *f-v* and *f-d* corresponding to each test condition. The acquired data are subsequently analyzed to characterize important properties of the MR-fluid damper[11].

Table 1 Test matrix of the MR-damper

Amplitude (a_m / mm)	Current (i_d / A)	Frequency (f / Hz)								
		0.1	0.5	1.5	2.5	5.0	7.5	10	12.5	15
2.5	0	×	×	×	×	×	×	×	×	×
	0.1	×	×	×	×	×	×	×	×	×
	0.2	×	×	×	×	×	×	×	×	×
	0.3	×	×	×	×	×	×	×	×	×
	0.4	×	×	×	×	×	×	×	×	×
12.5	0	×	×	×	×	×	×	×	×	
	0.1	×	×	×	×	×	×	×	×	
	0.2	×	×	×	×	×	×	×	×	
	0.3	×	×	×	×	×	×	×	×	
	0.4	×	×	×	×	×	×	×	×	
25	0	×	×	×	×	×	×	×		
	0.1	×	×	×	×	×	×	×		
	0.2	×	×	×	×	×	×	×		
	0.3	×	×	×	×	×	×	×		
	0.4	×	×	×	×	×	×	×		
50	0	×	×	×	×	×				
	0.1	×	×	×	×	×				
	0.2	×	×	×	×	×				
	0.3	×	×	×	×	×				
	0.4	×	×	×	×	×				
75	0	×	×	×	×					
	0.1	×	×	×	×					
	0.2	×	×	×	×					
	0.3	×	×	×	×					
	0.4	×	×	×	×					

2.2 Symmetric hysteretic *f-v* characteristics

The force-velocity (*f-v*) characteristics measured under a few selected excitation conditions are initially analyzed to build an understanding the dynamic behaviour of the MR-damper. Figs.3 to 5 illustrates a group of typical hysteretic *f-v* characteristics measured under selected harmonic excitations and drive currents. The results show that the damping force strongly depends on both the drive current (i_d) and the damper velocity ($v_r = \dot{x}_r$), and behaviors nearly linear rise at low velocities in the pre-yield and force saturation at higher velocities in the post-yield, as evident in Fig.3. The transition between pre- and post-yield stages occurs around the velocity v_r=0.025 m/s for the candidate damper considered. The nonlinear damping properties are further dependent upon excitation frequency and amplitude, as illustrated in Figs.4 and 5, respectively. Fig.4 illustrates that the hysteresis loop increases with increasing frequency in a nearly linear manner for frequencies below 10 Hz, and exhibits stronger hysteresis at higher frequencies. In the passive mode (i_d=0), the damping force varies nearly linearly with velocity, particularly at frequencies above 5.0 Hz, and the change in the damping coefficient observed at the onset of post-yield tends to diminish under higher excitation. Application of a higher current (i_d≥0.3 A) and excitation frequency (f≥10 Hz) causes a slight asymmetry in the hysteresis loop, while

larger hysteresis width in compression could be attributed to possible mixing of gas in the MR-fluid, as shown in Fig.4b. The results shown in Fig.5 further illustrate that the increase of excitation amplitude results in larger increase of hysteresis width in the damping force.

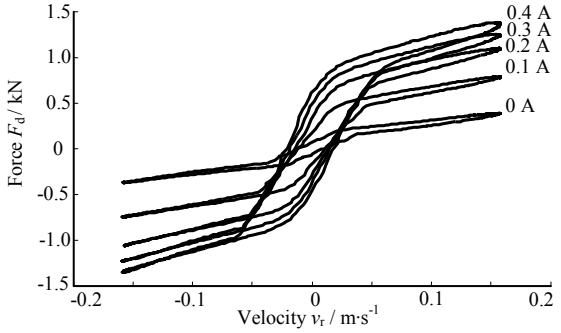

(a) f=0.5 Hz a_m=50 mm

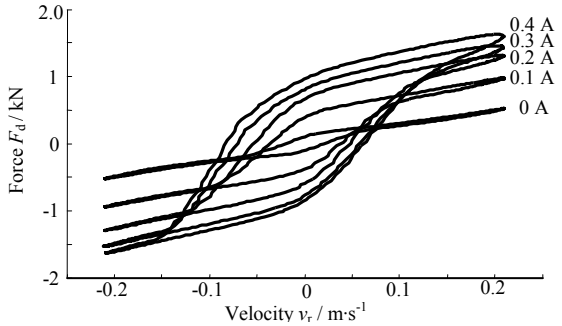

(b) f=2.5 Hz a_m=12.5 mm

Fig.3 Measured f-v characteristics of MR-damper under different drive currents and excitations

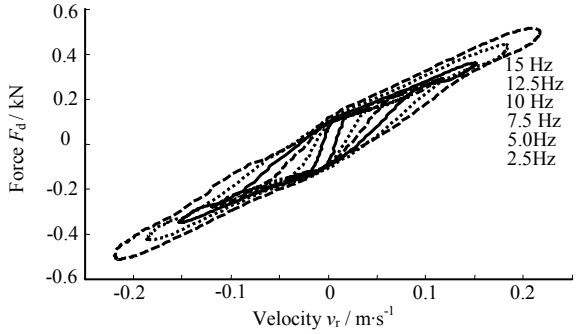

(a) i_d=0 A

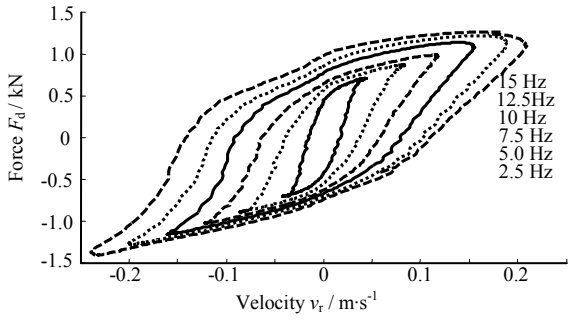

(b) i_d=0.2 A

Fig.4 Measured f-v characteristics of MR-damper under different excitation frequencies and drive current (a_m=2.5 mm)

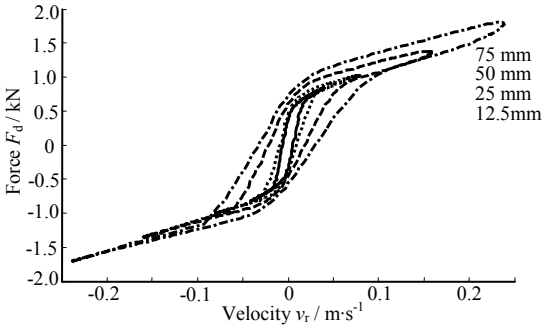

(a) i_d=0.2 A

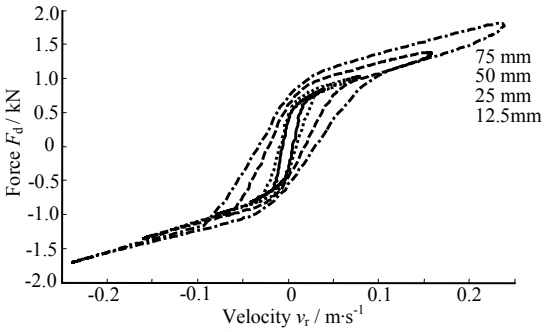

(b) i_d=0.4 A

Fig.5 Measured f-v characteristics of MR-damper under different excitation amplitudes and drive current (f=0.5 Hz)

The above experimental results reveals that the damping properties of the candidate damper strongly depend on the magnitudes of drive current, and excitation frequency and amplitude, and further reveals the essential dynamic behavior of the candidate MR-damper such as the controllable property, passive behavior, hysteretic phenomenon, which forms the basis for the generalized hysteretic f-v model synthesis proposed by the authors[5, 10].

3 Characterization of Asymmetric Hysteretic F-V Characteristics

The candidate MR-damper is designed to provide symmetric damping force in compression (v_r>0) and rebound (v_r<0). The vehicle suspension, however, are designed to realize asymmetric damping to achieve compromise among the conflicting ride, road-holding and directional control performances. It has been suggested that the ratio of rebound damping force to that in compression should be in the 3 to 5 range to realize better suspension performance. For this purpose, an asymmetric damping force generation (ADFG) algorithm[9] has been initially proposed by the authors and applied to experimental characterization of the asymmetric f-v characteristics from the symmetry MR-damper design, by integrating the algorithm within the current driver circuit. The proposed ADFG algorithm illustrates that the asymmetric damping properties of the symmetric candidate damper can be realized by limiting the drive current i_d to a lower value i_L during

compression, when the relative velocity of the piston is positive. The current is switched to a higher value i_H during rebound motion. Such an approach, however, would cause transient responses due to switching discontinuities around v_r=0, and an algebraic filtering technique without phase delay is integrated in the algorithm to suppress the current discontinuity. The asymmetric drive current of the MR-damper i_d is formulated as

$$i_d = \mathrm{M_p}(p,\xi,v_r)i_c \quad (1)$$

$$\mathrm{M_p}(p,\xi,v_r) = \frac{1+p}{2} + \frac{2}{\pi}[\mathrm{p}(v_r>0)\cup(v_r\le 0) - \frac{1+p}{2}]\left|\tan^{-1}(\frac{\xi v_r}{v_m})\right| \quad (2)$$

where $\mathrm{M_p}$ is the multiplier of the proposed ADFG algorithm, v_m is the peak relative velocity, p is asymmetry factor of drive current ($0\le p\le 1$) and ξ is smoothing factor defining the slope of the *arctan* function ($\xi>0$).

By implementing the proposed ADFG algorithm into the driving current circuit of the experimental setup shown in Fig.2, the experiments are performed to characterize the asymmetric damping force under the test conditions summarized in Table 1, and using p=0 and ξ=2 in the modulation function[11]. This would yield i_L=0 and i_H=i_d. As an example, Fig.6 illustrates the measured asymmetric hysteretic *f-v* characteristics corresponding to the selected excitation conditions and i_d ranging from 0 to 0.3 A. The results show that the same candidate damper can provide asymmetric damping force in compression and rebound in continuous manner. The chosen parameters of the modulation function yield asymmetric damping force ratio (γ) in the order of 4, for low velocities. The ratio γ, however, diminishes under higher velocities as observed in Fig.6d. A γ value of approximately 2 is attained under i_d=0.3 A, which is partly attributed to the force limited behavior of the MR-damper.

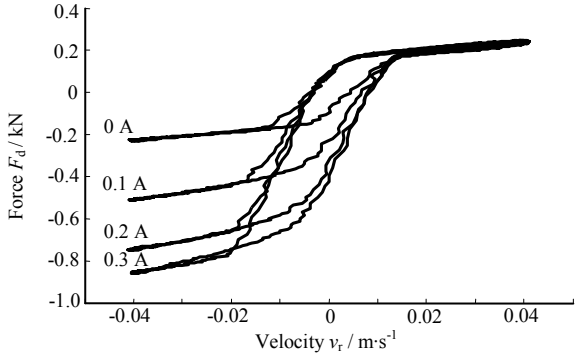

(a) f=0.5 Hz a_m=12.5 mm

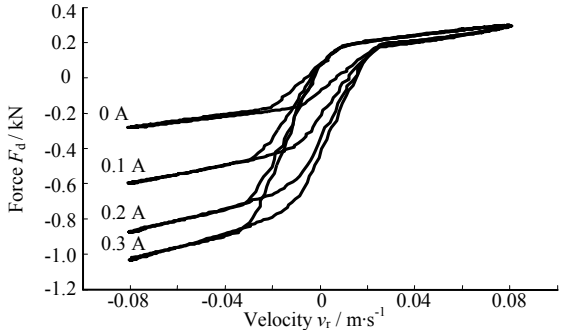

(b) f=0.5 Hz a_m=25 mm

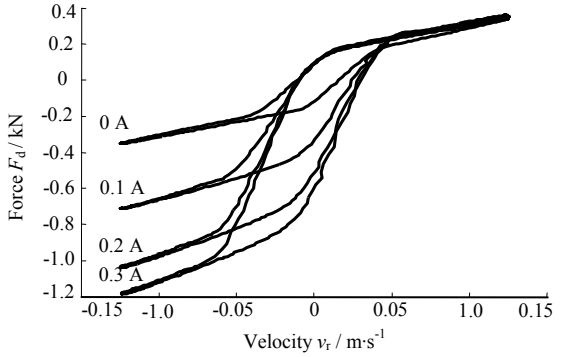

(c) f=1.5 Hz a_m=12.5 mm

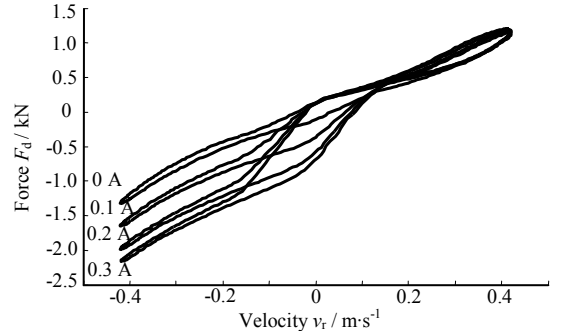

(d) f=2.5 Hz a_m=25 mm

Fig.6 Measured asymmetric *f-v* characteristics of the candidate MR-damper under different control conditions

5 Gnneralized Hysteretic F-V Model

The available test damper provided only symmetric damping force in rebound and compression due to the symmetric nature of the applied current. Furthermore, the reported models of the MR-damper, invariably, characterize the symmetric characteristics as a function of the piston velocity, while the current dependence is mostly ignored[1-4]. The vehicle suspension systems, however, are generally designed with asymmetric damping characteristic to achieve a better compromise among different conflicting performance measures. The conventional suspension dampers provide higher rebound damping to suppress wheel velocity in the upward direction when compared to that in the downward direction. The model synthesis of the symmetric damper[5] can be easily extended to characterize the asymmetric

hysteretic damper properties[10]. The generalized hysteretic *f-v* model is formulated as

$$F_{\mathrm{d}}(v_{\mathrm{r}},i_{\mathrm{d}})=\begin{cases} C_i(F_{\mathrm{t}}\dfrac{1-\mathrm{e}^{-a(v_{\mathrm{r}}+v_{\mathrm{h}}+v_{\mathrm{b}})}}{1+\mathrm{e}^{-a(v_{\mathrm{r}}+v_{\mathrm{h}}+v_{\mathrm{b}})}}-F_{\mathrm{b}})(1+k_{\mathrm{vc}}|v_{\mathrm{r}}|) & v_{\mathrm{r}}\ge 0 \\ C_i(F_{\mathrm{t}}\dfrac{1-\mathrm{e}^{-a(v_{\mathrm{r}}+v_{\mathrm{h}}+v_{\mathrm{b}})}}{1+\mathrm{e}^{-a(v_{\mathrm{r}}+v_{\mathrm{h}}+v_{\mathrm{b}})}}-F_{\mathrm{b}})(1+k_{\mathrm{ve}}|v_{\mathrm{r}}|) & v_{\mathrm{r}}<0 \end{cases} \quad (3)$$

The formulation can characterize both symmetric and asymmetric hysteretic *f-v* characteristics of the MR-damper, presented in Figs.3-6. The model involves feature parameters (F_{t}, F_{b}, v_{h}, v_{b}, α, k_{vc}, k_{ve}) that are dependent not only on the nature of excitation v_{m}, but also on the drive current i_{d}. The transition force F_{t}, the current dependent function C_{i}, the constant α, the zero-force velocity intercept v_{h}, the force offset F_{b}, the velocity offset v_{b}, the high velocity linear rise coefficients k_{ve} and k_{vc} are expressed as

$$F_{\mathrm{t}}=\mathrm{F}_0(1+\mathrm{e}^{a_1 v_{\mathrm{m}}}) \quad (4)$$

$$C_{\mathrm{i}}(i_{\mathrm{d}})=1+\frac{\mathrm{k}_2}{1+\mathrm{e}^{-a_2(i_{\mathrm{d}}+\mathrm{I}_0)}}-\frac{\mathrm{k}_2}{1+\mathrm{e}^{-a_2\mathrm{I}_0}},\quad C_{\mathrm{i}}(i_{\mathrm{d}})\ge 1 \quad (5)$$

$$a=a_0/(1+k_0 v_{\mathrm{m}}) \quad (6)$$

$$v_{\mathrm{h}}=\mathrm{sgn}(\ddot{x}_{\mathrm{r}})\,\mathrm{k}_4\,v_{\mathrm{m}}(1+\frac{\mathrm{k}_3}{1+\mathrm{e}^{-a_3(i_{\mathrm{d}}+\mathrm{I}_1)}}-\frac{\mathrm{k}_3}{1+\mathrm{e}^{-a_3\mathrm{I}_1}}) \quad (7)$$

$$F_{\mathrm{b}}=\mathrm{k}_5\,c_{\mathrm{i}}F_{\mathrm{t}} \qquad v_{\mathrm{b}}=\mathrm{k}_6\,v_{\mathrm{mt}} \quad (8)$$

$$k_{\mathrm{ve}}=\mathrm{k}_{1\mathrm{e}}\mathrm{e}^{-a_4 v_{\mathrm{m}}} \qquad k_{\mathrm{vc}}=\mathrm{k}_{1\mathrm{c}}\mathrm{e}^{-a_4 v_{\mathrm{m}}} \quad (9)$$

$$v_{\mathrm{m}}=\sqrt{(\dot{x}_{\mathrm{r}})^2-\ddot{x}_{\mathrm{r}}x_{\mathrm{r}}} \quad (10)$$

The proposed hysteretic *f-v* model can be used to describe both symmetric and asymmetric hysteretic *f-v* characteristics of the MR dampers as a function of the applied current and excitation condition. The model requires identification of a total of 16 parameters (F_0, I_0, I_1, a_0, a_1, a_2, a_3, a_4, k_0, $\mathrm{k}_{1\mathrm{c}}$, $\mathrm{k}_{1\mathrm{e}}$, k_2, k_3, k_4, k_5, k_6) from the measured data for the asymmetric characteristics, and can be simplified to characterize the symmetric *f-v* characteristics by letting $\mathrm{k}_5=\mathrm{k}_6=0$ and $\mathrm{k}_{1\mathrm{c}}=\mathrm{k}_{1\mathrm{e}}$. The damping force characteristics in the passive hysteretic mode can also be derived by letting $\mathrm{k}_2=0$, $\mathrm{k}_3=0$, $a_2=0$, $\alpha_3=0$, $\mathrm{I}_0=0$ and $\mathrm{I}_1=0$, and the proposed model can be further simplified to yield the mean *f-v* characteristics of the MR-damper by letting $\mathrm{k}_4=0$ ($v_{\mathrm{h}}=0$). It should be noted that the proposed generaliaed hysteretic *f-v* model has a little difference from that in the force offset parameter formulation F_{b} in[10].

5 Parameter Identification and Model Validation

A series of laboratory tests have been performed to characterize the dependence of hysteretic damping force of a MR-damper on the excitation frequency and stroke, and the drive current. The measured data are used to identify the parameters of the generalized symmetric and asymmetric hysteretic *f-v* model of the MR-damper, so as to demonstrate the effectiveness of the proposed model by comparing the simulation results with the measured data over a wide range of excitation parameters and magnitudes of drive current.

5.1 Model Parameter Identifications

The generalized hysteretic *f-v* model synthesis in conjunction with the measured data for the symmetric and asymmetric damping characteristics are used to identify the model parameters. In order to characterize the damping properties over wide ranges of applied current and excitation condition, a cost function U is formulated to incorporate the squared errors corresponding to different test conditions[11].

$$U=\sum_{l=1}^{L}\sum_{k=1}^{K}\sum_{j=1}^{J}[F(i_{\mathrm{d}},v_{\mathrm{r}})_{j,k,l}-F_{\mathrm{d}}(i_{\mathrm{d}},v_{\mathrm{r}})_{j,k,l}]^2 \quad (11)$$

where $F_{(j,k,l)}$ is the magnitude of measured damping force corresponding to j^{th} coordinate of the hysteron loop, k^{th} current and l^{th} frequency. $F_{\mathrm{d}(j,k,l)}$ is the corresponding damping force computed from the model. J, K and L define the levels of data points, currents and frequencies considered in the squared sum error function U.

The error function is derived upon considering the steady-state responses over a single cycle. A total of 360 data points are considered within each hysteresis loop derived for 5 different levels of current (K=5: 0, 0.1, 0.2, 0.3, and 0.4 A) and different excitation frequencies, for the symmetric *f-v* model parameter identification. The consideration of these frequencies for a given excitation magnitude provides a reasonable range of the piston velocity. The optimization function available within the MATLAB optimization toolbox (*fminunc*) is used to solve the minimization problem defined in Eq.(11). A number of inequality constraints for the model parameters are defined to ensure feasible solution: $a_{\mathrm{i}}\ge 0$ (i=1,…,4), $\mathrm{k}_{\mathrm{i}}\ge 0$ (i=1,…,6), and $\mathrm{F}_0>0$, while k_4, I_0 and I_1 were arbitrary values.

Owing to the strong dependence of the hysteretic forces in the symmetric and asymmetric modes on the peak velocity and thus the excitation frequency, the error minimization is performed for two different ranges of excitation frequencies for the symmetric *f-v* model parameter identification. The different model parameters are thus identified for the low and high frequency ranges in the 0.5 to 5.0 Hz and 5.0 to 15 Hz, respectively. A total of 4 different frequencies (J=4: 0.5, 1.5, 2.5 and 5.0 Hz) are considered for low frequency excitation, while those for the high frequency involved 5 different frequencies (J=5: 5, 7.5, 10, 12.5 and 15 Hz). For the asymmetric model, the parameter identification is limited to the low frequency only (J=2: 0.5 and 1.5), and 4 different levels of current are considered (K=4: 0, 0.1, 0.2 and 0.3).

Tables 2 and 3 summarize the parameters of the symmetric and asymmetric models identified from the measured data. The results presented for the symmetric model show that parameters related to the current dependence of the damping force (k_2, a_2, I_0), width of the hysteresis loop (k_3, a_3, I_1), transition force (a_1) and high velocity linear rise (k_1, a_4) are strongly influenced by the excitation frequency range. The low velocity behavior is relatively insensitive to the excitation frequency. This is evident from comparable values of the seal friction force (F_0) and low velocity rise parameter (a_0) under the two frequency ranges. The results presented for the asymmetric model show that parameters related to the low velocity behavior is almost the same as those of the symmetric model at low frequency range, which are the seal friction force (F_0), low velocity rise parameter (a_0) and hysteresis width parameter (k_4).

Table 2 Identified symmetric model parameters of the candidate MR-damper

Parameter	Frequency (Hz)		Parameter	Frequency (Hz)	
	0.5-5	5-15		0.5-5	5-15
a_0	992.985	988.967	k_0	125.987	177.249
a_1, s/m	5.197	4.477	k_1	11.2	9.486
a_2, A^{-1}	7.258	12.757	k_2	9.244	4.355
a_3, A^{-1}	6.635	10.137	k_3	9.186	17.781
a_4 , s/m	7.504	5.501	k_4	-0.119	-0.156
I_0, A	0.079	-0.082	F_0,	68.506	70.921
I_1, A	0.267	0.165			

Table 3 Identified asymmetric model parameters of the candidate MR-damper

Parameter	Asymmetry	Parameter	Asymmetry
a_0	995.499	k_{1c}	16.877
a_1, $(m/s)^{-1}$	1.417	k_{1e}	4.673
a_2, A^{-1}	5.225	k_2	10.61
a_3, A^{-1}	2.441	k_3	10.666
a_4 , $(m/s)^{-1}$	2.383	k_4	-0.125
I_0, A	0.268	k_5	0.269
I_1, A	1.131	k_6	0.453
k_0	177.51	F_0, N	79.92

5.2 Validation of symmetric *f-v* model

The proposed symmetric hysteretic *f-v* model is further analyzed under a wide range of excitation conditions and magnitudes of drive current. The simulation results are compared with the measured data to evaluate the effectiveness of the proposed model. Figs.7-9 shows comparisons of simulation results in terms of *f-v* characteristics with the measured data under a number of the test conditions, as examples, to demonstrate the validity of the proposed model. Fig.7 illustrates the comparisons under different drive currents (i_d=0 to 0.4 A) and two different excitation conditions (f=1.5 and 2.5 Hz; a_m=12.5 mm). Fig.8 shows comparisons of results under different excitation amplitudes in the 2.5 to 50 mm range, and frequencies in the 0.5 to 2.5 Hz range, while the applied current is held fixed (i_d=0.2 A). Fig.9 further illustrates the comparison of the model responses corresponding to higher frequency excitations with the measured data. The figure illustrates the model validity over the entire range of applied current (i_d=0 to 0.4 A) and excitation frequencies in the 5.0 to 15 Hz range, while the displacement amplitude is held as 2.5 mm. The model results follow trends similar to those observed in the measured data, correlate reasonably well with the measured data under lower currents and excitation frequencies.

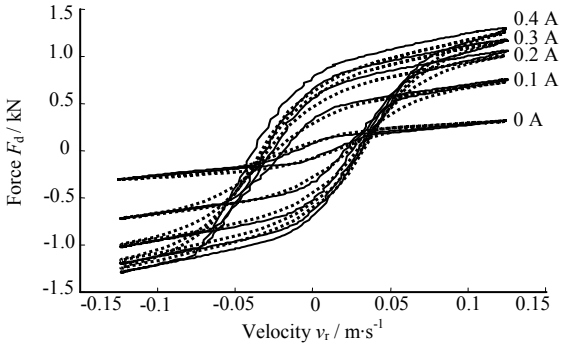

(a) f=1.5 Hz

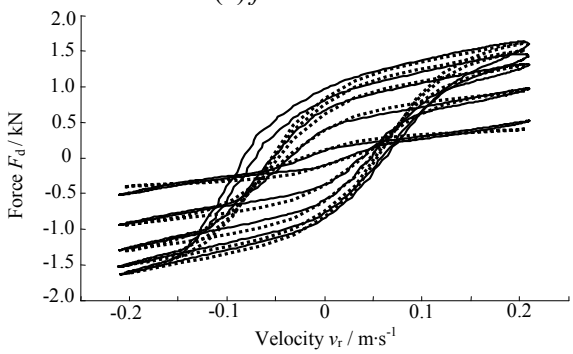

(b) f=2.5 Hz

Fig.7 Comparisons of symmetric model results with the measured data under different applied currents and excitation frequencies (a_m=12.5 mm)

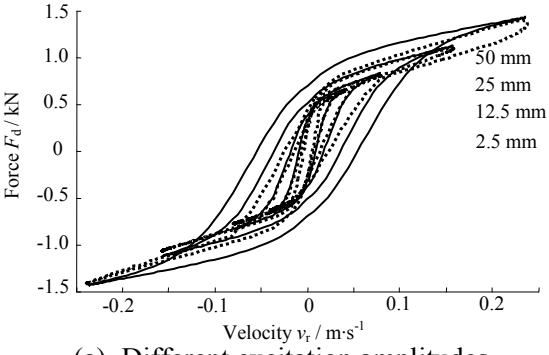

(a) Different excitation amplitudes, f=0.5 Hz

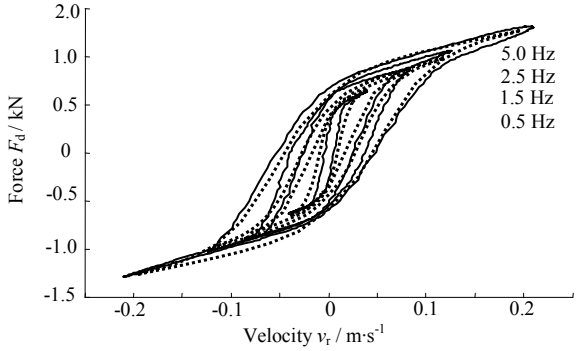

(b) Different frequencies, a_m=12.5 mm

Fig.8 Comparisons of symmetric model results with the measured data for fixed current (i_d=0.2 A)

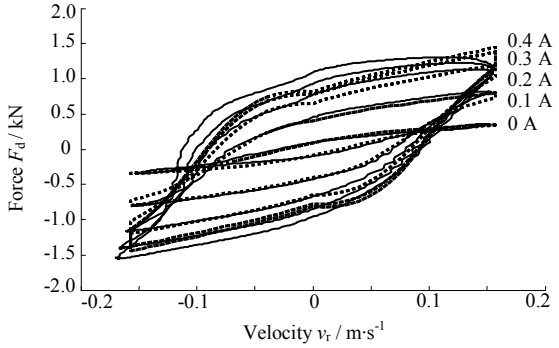

(a) Applied current: f=10 Hz a_m=2.5 mm

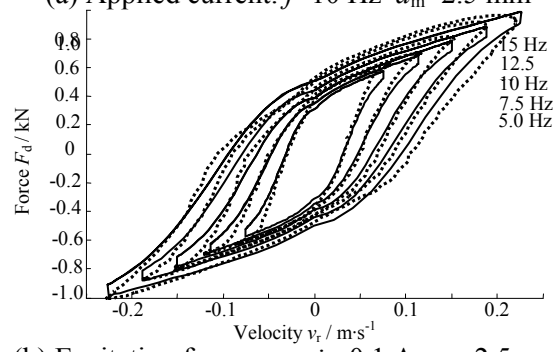

(b) Excitation frequency: i_d=0.1 A a_m=2.5 mm

Fig.9 Comparisons of symmetric model results with the measured data under higher frequency excitations

The above results generally show reasonably good agreements between the symmetric model results and the test data over the entire range of test conditions considered, with the exception of those attained at high frequencies.

5.3 Validation of asymmetric *f-v* model

The proposed asymmetric hysteretic *f-v* model is further analyzed under selected ranges of excitations and drive currents. The simulation results are compared with the measured data to demonstrate the validity of the proposed model. Fig.10 illustrates the comparisons of the model results with the measured data under different drive currents (i_d=0 to 0.4 A) and low frequency excitations (f=0.5 and 1.5 Hz; a_m=12.5 and 25 mm). The comparisons of model results with the measured data generally show reasonably good agreements between the model results and the test data over the range of test conditions considered.

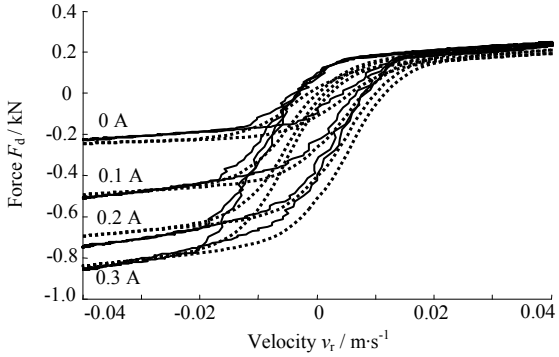

(a) f=0.5 Hz a_m=12.5 mm

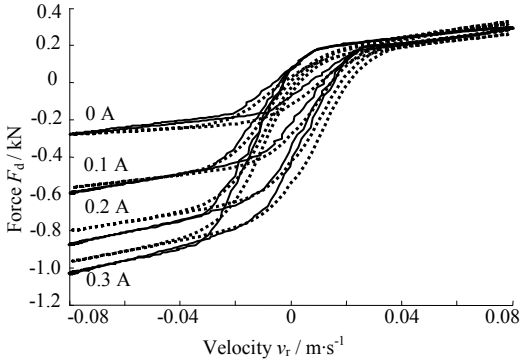

(b) f=0.5 Hz a_m=25 mm

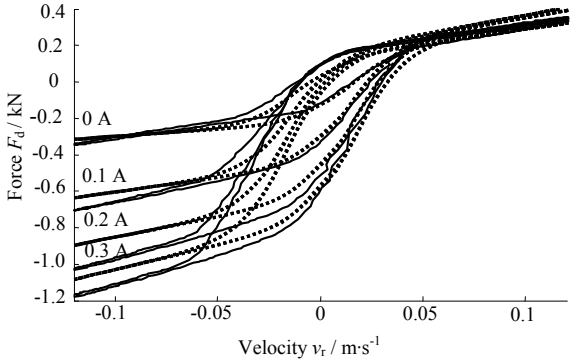

(c) f=1.5 Hz a_m=12.5 mm

Fig.10 Comparisons of asymmetric model results with the measured data under low frequency excitations and applied current

The above results show reasonably good agreements between the measured data and the asymmetric model results, irrespective of the applied current and excitation conditions within the lower frequency range.

6 Conclusion

Extensive laboratory measurements are performed to characterize the symmetric and asymmetric hysteresis force properties of a MR-damper under a wide range of drive current and excitation conditions (frequency and stroke). The proposed asymmetric damping force generation (ADFG) algorithm is used to generate the asymmetric damping force in compression and extension for the symmetric MR-damper, and a generalized model is proposed to

characterize the hysteretic *f-v* characteristics of the controllable symmetric and asymmetric MR dampers. Simulations are performed to assess the effectiveness of the proposed model synthesis and results obtained under wide range of simulation conditions are compared with those obtained from the measured data. The results show reasonably good agreements between the simulation results and the measured data, irrespective of the excitation conditions and control current. It is thus concluded that the proposed model can effectively describe the nonlinear symmetric and asymmetric hysteretic dynamic properties of the controllable MR dampers, and can thus be effectively used to synthesize the optimal semi-active controller for implementation in vehicle suspension.

References:

[1] Stanway R, Sproston J L, and EI-Wahed A K. Application of electro-rheological fluids in vibration control: a survey. J. of Smart Materials and Structures, 1996, 5(4): 464-482.

[2] Spencer B F, Dyke D J, Sain K M, and Carlson J D. Phenomenological model of a magneto-rheological damper. J. of Eng. Mech., 1997, 123(3): 230-238.

[3] Wereley N M, Pang L. Nondimensional analysis of semi-active electro-rheological and magneto-rheological dampers using approximate parallel plate models. J. of Smart Materials and Structures, 2000, 7: 732-743.

[4] Lee H S and Choi S B. Control and response characteristics of a magneto-rheological fluid damper for passenger vehicles. J. of Intelligent Material Systems and Structures, 2000, 11(1): 80-87.

[5] Wang E R, Ma X Q, Rakheja S, and Su C Y. Modeling hysteretic characteristics of an MR-fluid damper. Procs. of the Institution of Mechanical Engineers, J. of Automobile Engineering, 2003, 217(D7): 537–550.

[6] WANG E R, YING L, WANG W J, et al. Semi-active control of vehicle suspension with MR-damper: Part I-Controller synthesis and evaluation [J]. Chinese J. of Mechanical Engineering, 2007. (In press)

[7] WANG E R, YING L, WANG W J, et al. Semi-active control of vehicle suspension with MR-damper: Part II-Evaluation of suspension performance [J]. Chinese J. of Mechanical Engineering, 2007. (In press)

[8] WANG E R, YING L, WANG W J, et al. Semi-active control of vehicle suspension with MR-damper: Part III-Experimental validation [J]. Chinese J. of Mechanical Engineering, 2007.(In press)

[9] WANG E R, YE B M, CHEN Y S, et al. Research on generation of asymmetric f-v characteristics from symmetric MR-damper [J]. Chinese J. of Mechanical Engineering, 2006, 19(2): 239-244.

[10] WANG E R, MA X Q, RAKHEJA S, et al. Generalized asymmetric hysteresis model of controllable magneto-rheological damper for vehicle suspension attenuation. Chinese J. of Mechanical Engineering, 2004，17(2) :301-305.

[11]WANG E R. Syntheses and analyses of semi-active control algorithms for a magneto-rheological damper for vehicle suspensions [D]. Montreal, Canada, Concordia University, 2005.

[12]Carrera web site, http://www.carrerashocks.com, 2002.